Int J Environ Res (2022) 16:26
https://doi.org/10.1007/s41742-022-00405-w

RESEARCH PAPER

Synthesis and Characterization of Nano-$CoFe_2O_4$ Ferrite: Application to the Adsorption of AG25 Dye in Aqueous Solution

Ali Belhaine[1] · Fatiha Abdelmalek[1] · Abdelmadjid Rais[1] · Kamel Taibi[2] · Ahmed Addou[1]

Received: 23 November 2021 / Revised: 7 March 2022 / Accepted: 15 March 2022 / Published online: 7 April 2022

Abstract

Nano spinel of cobalt ferrite $CoFe_2O_4$ (NCF) has been synthesized by Sol–gel auto-combustion method and used as an adsorbent to remove Acid Green AG25 dye from aqueous solution. The NCF was investigated by XRD, Rietveld refinement, SEM coupled with EDX, VSM, FTIR and pH of the zero-point charge pH_{zpc}. The efficiency of the treatment was evaluated according to the characteristic parameters influencing the adsorption process: adsorbent dose, contact time, initial dye concentration, initial solution pH and temperature. The adsorption of AG25 followed pseudo-second order kinetic model. The equilibrium adsorption data fit to the Langmuir isotherm with a maximum capacity of 8.71 mg g^{-1}. Thermodynamic data revealed that the process was exothermic, spontaneous and a physisorption nature. Through the established adsorption process and magnetization measurements, a mechanism was proposed to highlight the idea that the nano spinel of cobalt ferrite material has both magnetic and electronic characteristics. NCF is an efficient adsorbent, low cost, easily synthesized and environmental friendly for removal AG25 from aqueous solution.

Graphical Abstract

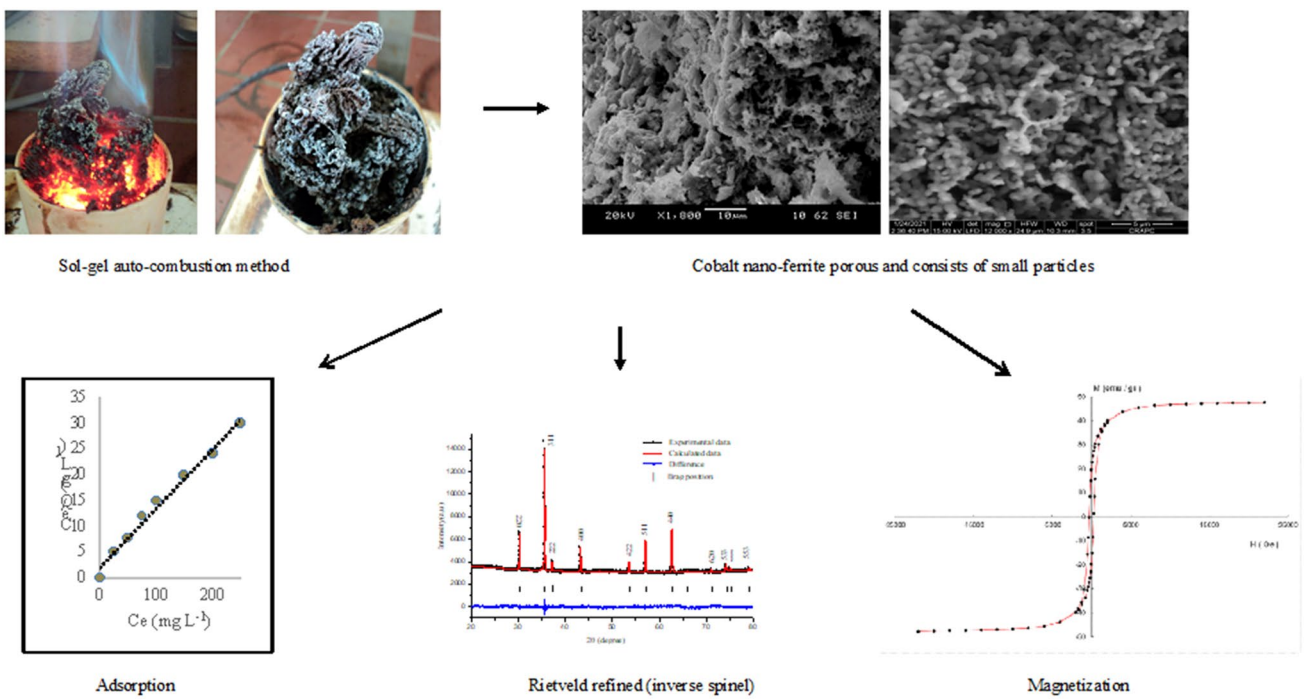

Extended author information available on the last page of the article

Highlights

- Adsorption of AG25 dye by nanoferrite $CoFe_2O_4$
- Synthèse by sol–gel auto-combustion
- mechanism study
- Combination between results of adsorption process and the proved magnetic properties
- $CoFe_2O_4$ material has both magnetic and electronic characteristics which can be beneficial for water pollution control

Keywords $CoFe_2O_4$ · Nanoparticles · Adsorption property · AG25 · Environmental friendly · Mechanism

Introduction

Water pollution remains a persistent problem in developing countries due to ineffective management, a lack of strict environmental laws and unsanitary social practices which lead to untreated effluents being discharged into water (Akhtar et al. 2021). Organic dyes have been largely utilized in several industries, including textiles, leather, plastic, paper, printing, cosmetics, pharmaceutical and many others (Lellis et al. 2019). The release of these compounds into the environment is undesirable because many dyes and their breakdown products are toxic and/or mutagenic to life (Singh et al. 2016).

To remove dyes from wastewater, various techniques have been developed such as coagulation, membrane filtration, advanced oxidation, biological treatment and adsorption (Rezai and Allahkarami, 2021; Ledakowicz et al. 2021; Pal 2017; Carolin et al. 2017; Qin et al. 2020; Benyekhou et al. 2020; Fast et al. 2017; Lellis et al. 2019).

The effective removal of organic pollutants from wastewater remains a challenge. In addition, recent studies have shown that nanoparticles synthesis using green methods may prove to be an attractive alternative (Manju et al. 2019; Aragaw and Bogale 2021; Varghese et al. 2019).

Spinel ferrite magnetic nanoparticles have been regarded as a promising adsorbent due to their high stability, high surface area and excellent magnetic characteristics at room temperature (Saravanathamizhan et al. 2021). The chemical and physical properties of these materials make them a field of great interest with broad application (Soltys et al. 2021). Currently, adsorption is considered to be a suitable technique since it has the advantage of using nanoparticles that are less low cost environmentally friendly, recyclable and industrially exploitable. Nanoferrites have these qualities and offer the advantage of being used as adsorbents for wastewater treatment (Pai et al. 2021; Hassan and Aly 2021; Manimozhi et al. 2020; Thakur et al. 2016; Akhtar et al. 2018; Gherca et al. 2013).

A number of methods have been developed to synthesis nanoferrite including sol–gel method, co-precipitation method and hydrothermal method (Kefeni et al. 2017; Naseri et al. 2012; Kumar et al. 2019Xiaoli et al. 2015). Among the various methods, the auto-combustion synthesis method has attracted attention because of its inexpensive precursors, simple manipulations and simple control of solution pH value during the chemical process (Moosavi et al. 2020).

Previous publications reported that magnetic separation technology, combined with the adsorption process, has been widely used for wastewater treatment (Kadirvelu et al. 2003).

The condition required to move from lab-scale application to an industrial scale, is the separation of adsorbent materials from treated water and avoiding secondary pollution. Non recyclability is expensive and may limit its applications on a large scale. The remedy for this inconveniency is to combine performance of sorption and magnetic separation processes for pollutant removal (Baig et al. 2021).

Acid Green 25 (AG25) acid also been known as Acid Green Anthraquinone or Alizarin Cyanine Green F has been selected for the present study. It was chosen as a model pollutant for its toxic and persistent properties (Sajjia et al. 2014; Soufi et al. 2021). Acid dyes which comprise the largest class of dye are anionic compounds used in the cosmetics, pharmaceutical and textile industries. Anthraquinone dyes are the most important after azo dyes. Wastewater from the textile industry is often very colourful and difficult to biodegrade. This pollution is currently perceived as a serious and significant nuisance (Shen et al. 2021; Samoila et al. 2015).

The objective of the present work is to explore the adsorption potential of cobalt ferrite nanoparticles $CoFe_2O_4$ (NCF), synthesized by auto-combustion method for the removal of AG 25 dye from an aqueous solution.

The microstructure, morphology and magnetic properties of as-synthesized $CoFe_2O_4$ were studied by infrared absorption spectrum (FTIR), X-ray diffraction (XRD), scanning electron microscope (SEM) and vibrating sample magnetometer (VSM) technique, respectively. Effects of

various parameters like contact time, solution pH, adsorbent dose were investigated. The experimental data for adsorption have been analyzed using the Langmuir and Freundlich isotherm. A global mechanism of the interaction AG25-NFC was proposed.

Materials and Methods

Preparation of $CoFe_2O_4$ Spinel Nanoparticles

The $CoFe_2O_4$ spinel nanoparticles was synthesized by sol–gel auto combustion method using analytical grade chemicals. Stochiometric amounts of $Fe(NO_3)_3.9H_2O$, $Co(NO_3)_2.5H_2O$ and citric acid $C_6H_8O_7.H_2O$ (Sigma Aldrich, > 99%), were weighed as citric acid/metal ion mole ratio of 1:1 and dissolved separately in a minimal amount of distilled water. The solutions were then mixed and the pH adjusted to be betwen 6 and 7 with constant stirring by adding a dilute solution of NH_4OH. This resulting solution was heated to 70 °C under a constant heating rate and continuous magnetic stirring to ensure good homogenization of the mixture. Around 100 °C, the solution started to boil and foam due to dehydration. Nearby 200 °C, the solution slowly changed into a viscous gel with further release of water molecules and thickening (clotting) of the gel. Subsequently, a reddish brown gas evolved which caused the gel to auto-combust with flame propagation producing a dry fluffly cobalt nanoferrite material. The black compound formed was ground in an agate mortar to a fine powder. It was then calcined for 6 h at 900 °C under a constant heating rate of 10 °C/min using a muffle furnace (Carbolite 1100) to remove any organic material.

Acid Green Dye (AG25)

The AG25 anthraquinone dye used of analytical grade, supplied by Acros Organics, greater than 99% purity. Its chamical formula is $C_{28}H_{22}N_2O_8S_2Na_2$ and its molar mass is 622.574 g mol^{-1}. The chemical structure of the molecule is given in Fig. 1. The stock solution of AG25 (30 mg L^{-1}) was prepared with distilled water and the concentrations used were obtained by dilution.

The removal rate $R(\%)$ was calculated using the following equation:

$$R(\%) = \frac{C_0 - C_e}{C_0} \times 100, \quad (1)$$

where C_o and C_e (mg L^{-1}) are the initial and final concentrations of AG25 in the supernatant, respectevely. The absorbance of the concentrations has been measured at $\lambda_{max} = 643$ nm using a UV/Vis spectrophotometer (OPTIZEN 2120).

Characterization of Nano-Ferrite of Cobalt Material

The characterization was carried out by the following techniques: DRX, SEM, VSM, Fourier Transform Infrared Spectroscopy (FTIR) and pH of the zero-point charge (pHzpc).

X-Ray Diffraction

The X-ray diffraction spectrum of $CoFe_2O_4$ has been obtained with a Panalytical X' Pert Pro diffractometer using CuKα radiation (λ1/4 1.5406 Å). The scan's range was kept the same $2\theta = 20°–100°$ using a step size of 0.01° with sample time of 10 s. The analysis was preformed by HighScore Plus® program (produced by PANalytical B.V. under license number 10003977) based on the Rietveld refinement method (Young 1996).

SEM

Scanning Electron Microscopie combined with Energy Dispersive X-ray (EDX) microanalysis is a technique that allows qualitative and quantitative surface analysis of inorganic materials. The morphology and nanostructure of the samples were analyzed by scanning electron microscopy an ASEM; JEOL JSM6360, coupled with an energy dispersive system (EDS, EDAX) for elementary composition analysis.

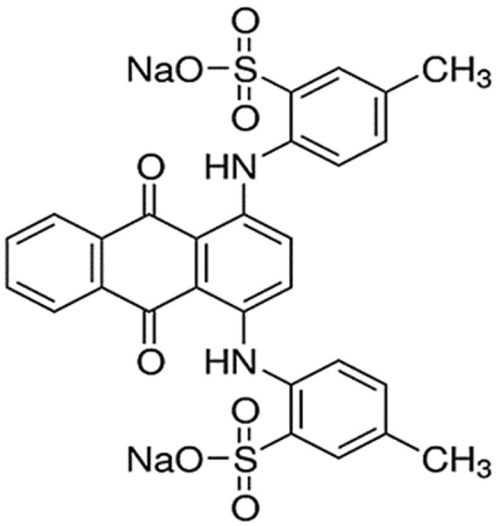

Fig. 1 Chemical structure of the AG25 dye

VSM Measurements

The magnetization measurements were carried out with a vibration sample magnetometer (VSM) of sensitivity 10^{-5} emu (Microsenze EZ9 brandt).

FTIR Spectroscopy

The samples were prepared in the form of KBr pellets with 1% powder (pressed in a cylindrical disc at 10 tons/cm^2 by hydraulic press) and fixed on a support in the spectrophotometer measurement chamber. IR spectra was recorded from 400 to 1000 cm^{-1} using a Shimadzu Fourier Transform Infrared Spectrophotometer IR prestige 21 with a resolution of 4 cm^{-1}.

pH of the Point of Zero Charge (pHpzc)

The pHpzc has been determined by the method of Noh and Schwarz (1989). Serials of 0.15 g of nanoferrite were introduced into Erlenmeyer flasks containing 50 mL of 10^{-2} M of NaCl. The initial pH of the solution was varied from 2 to 12 using HCl (10^{-1} M) or NaOH (10^{-1} M). The suspensions are mechanically stirred and maintained at room temperature. After 48 h of stirring, the final pH is mesasured. The latter is plotted as a function of the initial pH. The pH which corresponds to the point of intersection with the line $pH_{final} = pH_{initial}$ is the pH_{pzc}.

Adsorption

All the adsorption experiments were carried out at natural pH of 5.24. The batch experiments consisted to evaluate the AG25 dye removal at equilibrium and to calculate the effect of pH, adsorbent dose and temperature. The initial concentration of 30 mg L^{-1} was adopted to follow the evolution of adsorption as a function of the contact time from 1 to 40 min. These experiments were conducted at 20 °C with a mass of NCF and stirred at 400 rpm in 25 mL solution for a specified time. The NCF-AG25 mixture was centrifuged at 400 rpm for 10 min to separate the adsorbent from the aqueous solution. The absorbance of the filtrate was measured by UV/Vis spectrophotometry (OPTIZEN 2120) at 643 nm. The adsorption rate R (%) of the dye was calculated by Eq. (1):

The adsorption capacity (q) is given by the following equation:

$$q = \frac{(C_0 - C_e)V}{m}, \quad (2)$$

where, q (mg g^{-1}) is the amount of the dye adsorbed, V (L) is the volume of the dye solution and m (g) is the mass of NCF.

Adsorption Parameters

The parameters influencing the adsorption process were studied: adsorbent dose, contact time, initial dye concentration, initial solution pH and temperature.

Equilibrium Time

The adsorption equilibrium time has been determined as a function of the adsorbent-adsorbate contact time. The experiments were carried out in a batch system. The equilibrium time was calculated by increasing the stirring time from 5 to 120 min while mainyaining the pH at 5.24 (natural pH of the solution). Solutions of 25 ml of AG25 (30 mg L^{-1}) were added to 0.5 g of NCF. The mixture was stirred at 20 °C with mechanical strirrers (Wisestir HS-30D) at 400 rpm. After the equilibrium, the suspension was separated by centrifugation (Centurion Scientific- Ltd) for analysis of the dye concentration at 643 nm.

Adsorbent Dose

The evaluation of the effect of the optimal amount of adsorbent was carried out with 25 mL of the AG25 solution (30 mg L^{-1}) to which different amounts of adsorbent ranging from 0.05 to 0.8 g L^{-1} were been added. The solutions were stirred for a time exceeding the adsorbate-adsorbent equilibrium time (100 min).

pH

To evaluate this effect, pH was observed within the pH range of 2–10. An optimum mass of 0.5 g of adsorbent was added to 25 mL of AG25 (30 mg L^{-1}) and stirred for 20 min at 20 °C.

Kinetic and Isotherms Studies

For the kinetic study, an initial concentration of at 30 mg L^{-1} was adopted to follow the evolution of adsorption as a function of contact time. 0.5 g of the adsorbent was added to 25 ml of AG25 solution for initial concentrations of 50 to 500 mg L^{-1}. The mixture was stirred at a room temperature for the adsorbate-adsorbent equilibrium time (100 min) with mechanical stirrers at 400 rpm.

Adsorption Thermodynamic Parameters

0.5 g of the NCF is suspended with 25 mL of AG25 (30 mg L^{-1}) at natural pH (5.24). The Erlenmeyer flask containing the mixture is placed in a thermostat bath at different temperatures. Mechanical stirring ensures good dispersion and thermal homogeneity of the solution with mechanical stirriers (Wisestir HS-30D) at 400 rpm for 100 min at temperatures of 25, 30 and 40 °C. The solid–liquid separation is carried out by centrifugation using a centrifuge (Centurion Scientific-Ltd) at 6000 rpm for 10 min. The absorbance was determined at $\lambda_{max} = 643$ nm.

Results and Discussion

Physical and Magnetic Properties of Material

X-Ray Diffraction Analysis and Rietveld Refinement

Figure 2 shows the XRD pattern of $CoFe_2O_4$ powder. The refinement of the spectrum was indexed to peaks in space group *Fd3m* with planes: (220), (311), (222), (400), (422), (511), (440), (620), (533), (444), (553), thus proving the formation of single-phase cubic spinel structure. Note that all the reflection peaks are consistent with those reported earlier for $CoFe_2O_4$ (Joint Committee for Powder Diffraction Set (JCPDS) Card No. 86-6722). To model the XRD pattern peak profile, a pseudo-Voigt function was utilized with the oxygen positions ($x = y = z = u$) taken as free parameters. The cobalt and iron cations were in the Wickoff positions 8b and 16c, the oxygen ions in 32e special positions. To assess the Rietveld fittings quality, we used the reliability R-factors expected and weighted profile R_{exp} and R_{wp}, respectively which must be less than 10%. When the fitting parameters reached their minimum value, the goodness-of-fit $GoF = R_{wp}/R_{exp}$ must tend to one and the best fit to the experimental data is achieved (Cullity and Stroke 2013; Young and Wilse 1982).

Table 1 shows the typical atomic positions ($x = y = z$) of the cations, the oxygen position parameter u, the R-factors and the GoF. The experimental and calculated data as well as the difference between the two, thus confirming the reasonably good fit. The occupancies of the cations in tetrahedral (A) and octahedral (B) sites are constrained to preserve the stoichiometry of the prepared ferrites during the refinement. The resulting site occupancy factors (SOF) will enable to determine the stoichiometric coefficients for cations in A and B sites which are consistent with the spinel ferrites formula AB_2O_4 (Smith and Wijn 1959; Sickafus et al. 1999). Fractional atomic positions ($x = y = z$) at Wyckoff positions, site occupancy factors (SOF), fit R-factors expected and weighted profile, goodness of fit (GoF) and cations distribution at tetrahedral (A) and octahedral (B) sites of $CoFe_2O_4$ Furthermore, from Rietveld refinement conventional factors calculations, it can be seen that the cation distribution of $CoFe_2O_4$ and oxygen position revealed that the chemical structure is $(Co_{0.36}\ Fe_{0.64})\ [Co_{0.64}\ Fe_{1.36}]O_4$, with $u = 0.442$. Consequently, Co ions are both in tetrahedral and octahedral sites, which reveal $CoFe_2O_4$ is in partially inversed spinel structure comparable to nano-crystallite Mg-ferrite prepared using the sol–gel technique (Raghasudha et al. 2015) and normal crystallite Mg-ferrite prepared by the standard ceramic technique (Sabri et al. 2016).

The crystallite size L_{XRD}, of each sample was evaluated from the reflected diffraction peaks of the Rietveld refined profile using Scherrer's equation (Cullity 1978) as follwos:

$$L_{XRD} = \frac{k\lambda}{\beta.\cos\theta}, \tag{3}$$

where the constant $k = 0.89$, λ is the wavelength of the X-ray radiation (= 1.5406 Å), θ is the diffraction angle of the most intense peak (311) and β is its full width at half maximum in radian. The crystallite size L_{XRD} value was found to be 27.3 nm.

SEM Analysis

The SEM images presented in Fig. 3a at magnifications × 12,000 and × 1800 show that the cobalt nano-ferrite obtained by annealing at 900 °C is porous and consists of small particles, almost homogeneous in shape and size. The morphology is compact with pores and voids at the grains boundaries forming a medium of large agglomerates. The mean grain size, obtained through the analysis of the SEM micrographs (Fig. 3b), indicates that the grain size distribution histograms is about ~ 2.5 µm. The EDX spectrum shown in Fig. 4 confirms the qualitative and quantitative analysis corresponding to the synthetised composition of $CoFe_2O_4$.

Vibrating Sample Magnetometry (VSM)

The magnetizations versus magnetic field at room temperature of nano-sized ferrite powder sample are shown in Fig. 5. The magnetic parameters extracted from the Hysteresis loop, i.e. saturation magnetization (M_S), coercitive field (H_C), remanence (M_R) and squareness ratio $R = M_R/M_S$ are listed in the inset table. It is well known that the magnetic properties of nanosized crystallite of ferrites depend primarelly on the preparation method and the parameters of the technique (Hossain et al. 2018; Murugesan et al. 2014). For example, it has been reported that 16 nm nanosized cobalt ferrite prepared by co-precipitation gives a squareness ratio R of 27%,

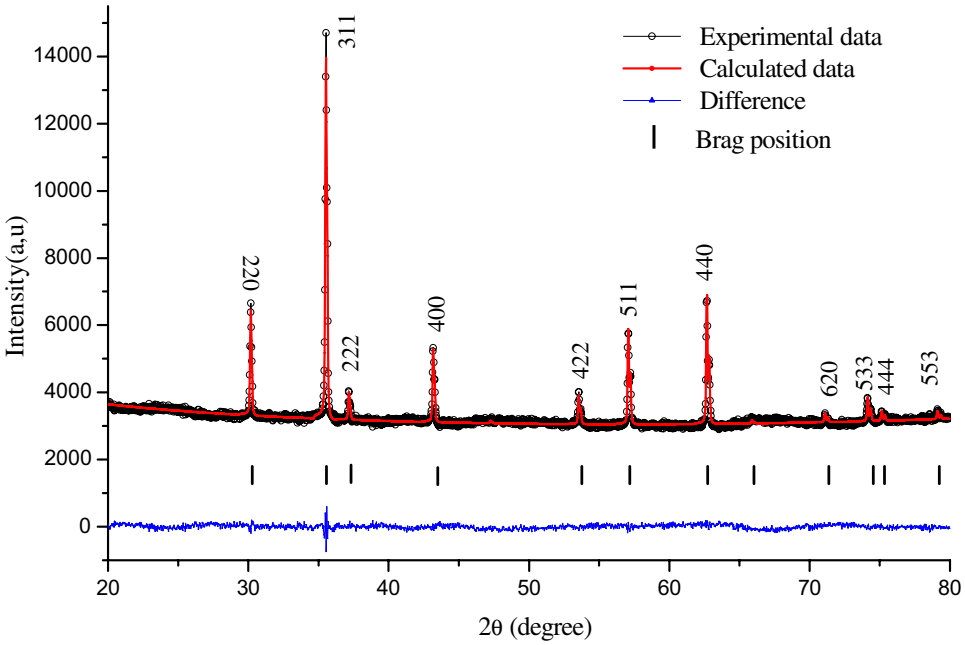

Fig. 2 Rietveld refined XRD patterns of $CoFe_2O_4$ at 900 °C

Table 1 Atomic positions and Wyckoff positions site of $CoFe_2O_4$

Atom	Wyck	S.O.F	*x*	*y*	*z*
O_1	32e	1.000	0.249	0.249	0.249
Fe_1	16c	0.680	0.000	0.000	0.000
Co_1	16c	0.320	0.000	0.000	0.000
Fe_2	8b	0.640	0.375	0.375	0.375

whereas 13 nm cobalt nano-ferrite prepared by polymeric precursor method (Mathew and Juang 2007) gives the value of 50%. Furthermore, some reports prove that crystallites of cobalt nano-ferrites having an *R* less than 50% interact magnetostatically whereas for those having an $R \geq 50\%$, the crystallite moments are randomly oriented and can undergo coherent ratios. Hence, in this work, the value of $R = 41\%$ may be attributed to magnetostatic interactions between crystallite grains. Moreover, it is reported that coercitivity depends entirely on the packing of the crystallite grains (Cullity and Graham 2009) and a comparative study between bulk Co-ferrite prepared by high temperature ceramic method and nano-crystalline Co-ferrite by low temperature auto-combustion (Murugesan et al. 2014) has shown that coercitivity is much higher for nano-ferrite by four factors. The obtaied value of Hc (299 Oe) may be related to the technique as well as the annealing temperature (900 °C) which have direct effect on domain structure, monocrystal size and anisotropy of the crystal (Qu et al. 2006).

$CoFe_2O_4$ – AG25 Interaction: FTIR Spectroscopy

The interaction between the nano-ferrite of cobalt and the AG25 dye was investigated by FTIR spectroscopy. Figure 6 shows the FTIR spectra of AG25, $CoFe_2O_4$ and $CoFe_2O_4$ – AG25.

In this study infrared spectroscopy confirms the spinel structure of the cobalt nanoferrite. Measurements in the 400–4000 cm^{-1} range show clearly the presence of two strong absorption bands ν_1 at 437 cm^{-1} and ν_2 at 556 cm^{-1} (Fig. 6a). The two normal modes of vibration are active in the range 400–700 cm^{-1}. The ν_1 absorption band is assigned to the stretching vibration mode of the metal–oxygen in octahedral B-sites and the ν_2 band is attribued to tetrahedral A-sites. The higher frequency of A-sites with respect to B-sites could be interpreted as due to shorter length of A-sites metal–oxygen bonds than B-sites length. NCF is exhibiting an inverse spinel where Co^{2+} ions and Fe^{3+} ions present at the octahedral and tetrahedral lattice sites respectively (Mostafa and Mai 2016). Moreover, reasonably good agreement of these frequency bands with Prabagar et al. [2021) who observed ν_1 at 462 cm^{-1} and ν_2 at 579 cm^{-1} for Cobalt nano- ferrite prepared using the sol–gel auto-combustion method and annealing at 600 °C, their crystallites size was found equal to 13.5 nm.

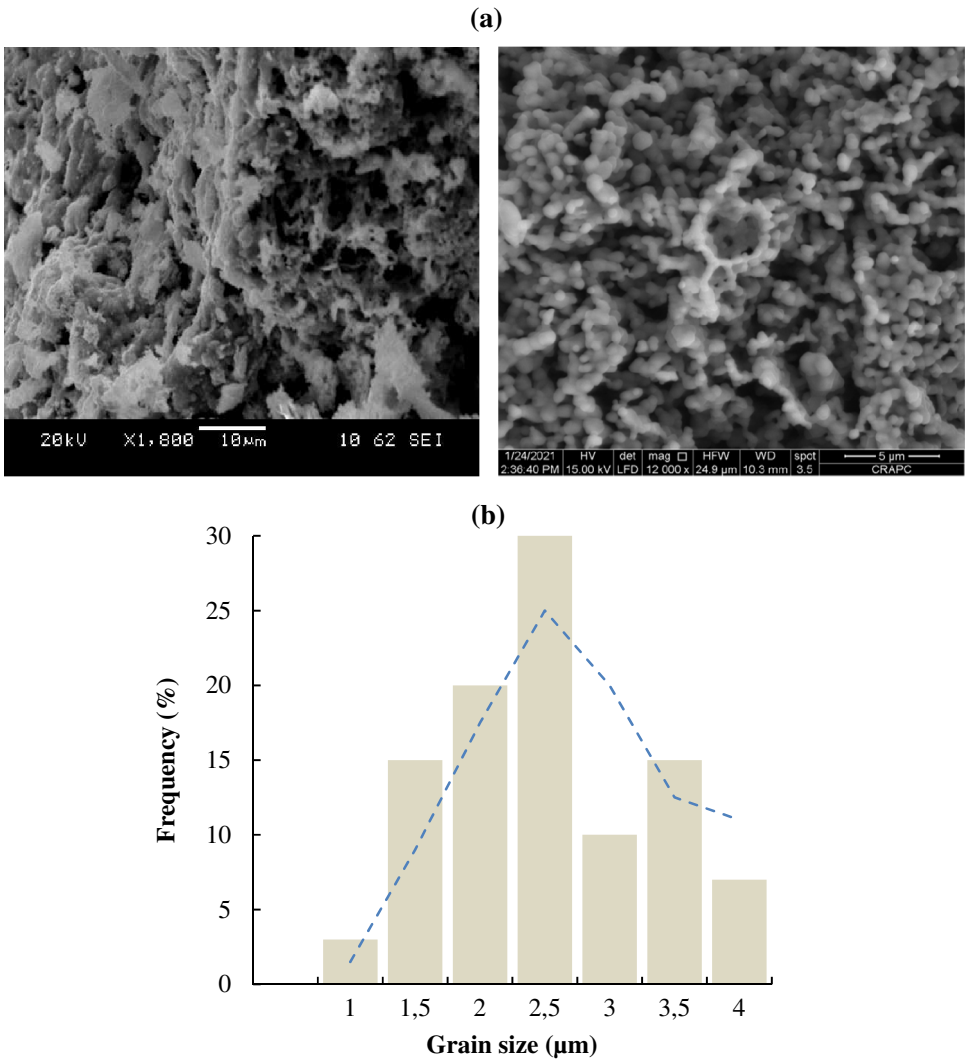

Fig. 3 SEM micrographs of: **a** $CoFe_2O_4$; and **b** $CoFe_2O_4$ annealed at 900 °C

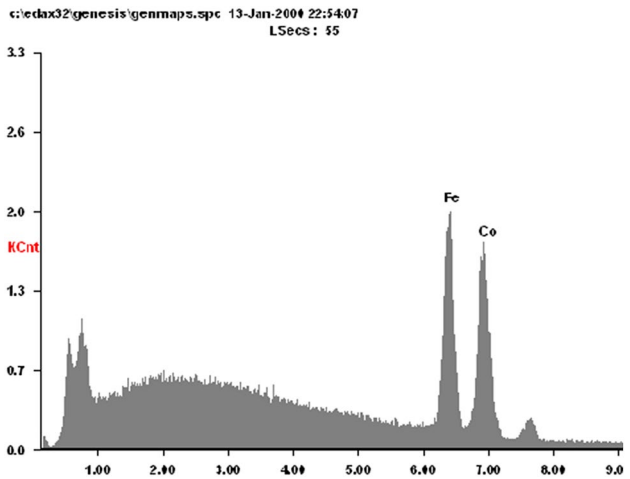

Fig. 4 EDX spectrum of $CoFe_2O_4$

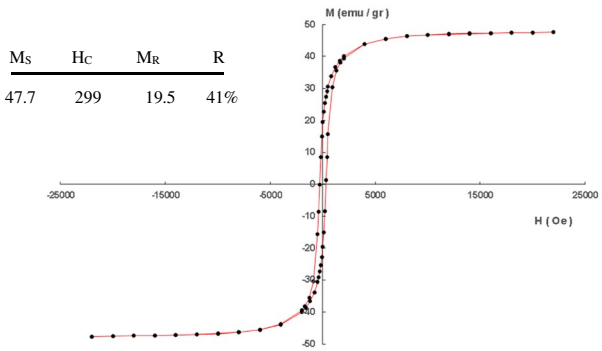

Fig. 5 Room temperature magnetization M versus magnetic field H of $CoFe_2O_4$

After interaction of AG25 by NCF (Fig. 6b), changes in the frequencies and intensities of the absorption bands could be observed for several functional groups. This observation may indicate the existence of an appropriate mechanism for the NCF-AG25 interation by means of an adsorption process through chemical bonding or Van der Waals forces (Mahmoodi et al. 2019). The study of the FTIR spectra allows to propose a mechanism based on the static electrostatic interaction as follws: the $-SO_3^{2-}$ ionic group can easily form attractive forces between AG25 and the positive surface charge of NCF. This type of attraction can be assimiled to a strong dipole force and makes the adsorption process stronger (Mahmoodi et al. 2018). Indeed, adsorption is widely interpreted by mechanisms such as: π–π interaction/stacking, hydrogen bonding and electrostatic interactions. As a result of this adsorption, the frequencies appeared at 437 and 556 cm^{-1} for NCF were shifted after adsorption to 451 and 563 cm^{-1} with a decrease in the intensity of the absorption band at 451 cm^{-1}. At this stage, it is possible to propose a mechanism as follows:

$$AG25 + H_2O \leftrightharpoons AG25^-_{aq} + 2H^+, \quad (4)$$

$$2NCF - OH^+_{surface} + AG25^-_{aq} \leftrightharpoons NCF - O - AG25. \quad (5)$$

The AG25 molecule, behaving like a Bronsted acid, decomposes in water giving two protons and a conjugate base ($AG25^-_{aq}$) to its sulphonate group $-SO_3^-$. Two NCF ($2NCF - OH^+_{surface}$ moleculs positively charged surface will combine with AG25 via these groups. This mechanism will be confirmed in the results announced later in this article.

By comparing with the FTIR spectrum of AG25 presented in Fig. 6c. More modifications after interaction are noticed as follows:

- Almost total disappearance of the 3470 cm^{-1} NH stretching bond,
- A decrease in intensity of the 2924 cm^{-1} CH asymmetric stretching (CH_2),
- A decrease in intensity of the 2855 cm^{-1} CH symmetric stretching (CH_2),
- A total disappearance of the 1504 cm^{-1} NH_2 bending,
- A shift from 1460 to 1456 cm^{-1} of the intense –COO asymmetric stretching absorption band,
- A shift from 1371 to 1377 cm^{-1} of –COO asymmetric stretching,
- A total disappearance of the 725 cm^{-1} CH_2 wagging.

The intensity variations of the different functional groups suggest that the interaction rise to adsorption between AG25 and NCF.

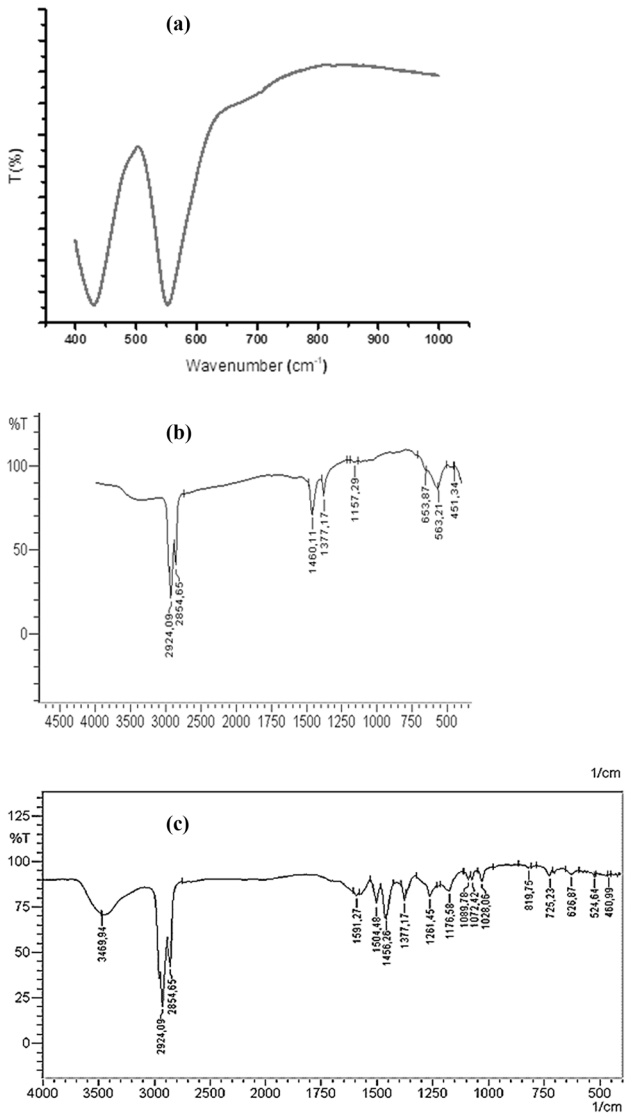

Fig. 6 Infrared spectrum of: **a** $CoFe_2O_4$; **b**: $CoFe_2O_4$-AG25 and **c** AG25

Adsorption: AG25/$CoFe_2O_4$ System

pH_{pzc}

The pH of the point of zero charge (pH_{pzc}) is an important parameter used in the estimation of the acid–base effect when electrostatic forces are involved in the mechanism of adsorption (Kosmulski 2017). To summarize the adsorption mechanism and the influence of pH, it would therefore be interesting to determine the Point of Zero Charge (PZC) of the adsorbent. In all cases, the adsorption of cations is favored at $pH > pH_{PZC}$ and the adsorption of anions is favored at $pH < pH_{PZC}$.

The pH_{pzc} corresponds to the pH value for which the charge on the surface of adsorbent is zero. It is the pH of an aqueous solution in which a solid exists under a neutral electrical potential. Figure 7 shows that the pHpzc is equal to 6.1. When the pH is > 6.1, the surface of the adsorbent, by loosing protons, becomes negatively charged and disfavours the attracation of AG25, which is an anionic dye, due to the decrease of the electrostatic attraction force. For pH < 6.1, there is an increase in the attraction force because of the increase in the positive charge of the adsorbent surface.

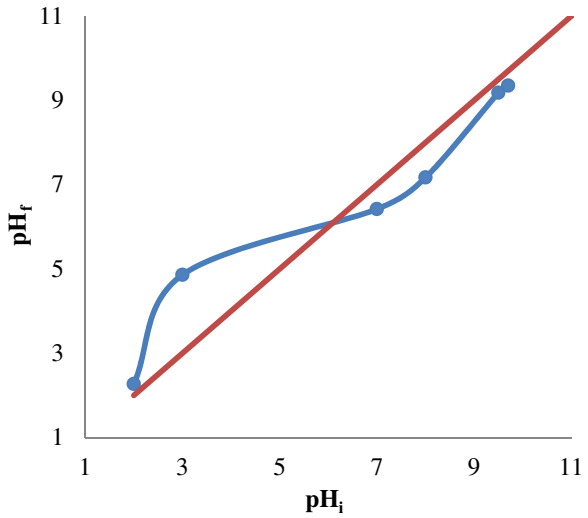

Fig. 7 pHpzc of $CoFe_2O_4$

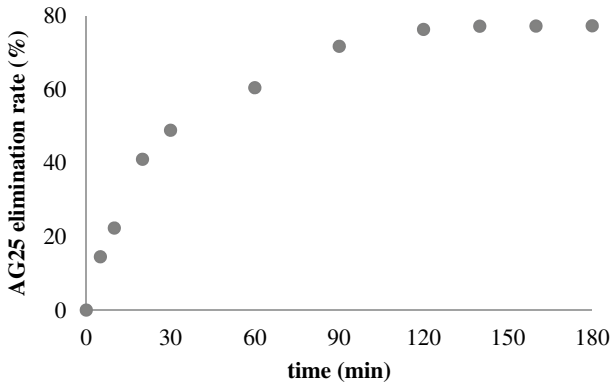

Fig. 8 Discoloration rate of AG25 solution as a function time

Adsorption Parameters

Equilibrium Time Figure 8 shows that the equilibrium time is of 120 min for a maximum elimination rate of 75% of dye. The instantaneous profile of the concentration of AG25 solution obtained experimentally shows an equilibrium rate followed by a saturation step which stabilizes nearby 100 min. Adsorption can be controled by the transfer rate of the adsorbate through the outer liquid film and/or diffusion of the solute inside the adsorbent particle (Zaviska et al. 2009; Wang and Chen 2020). The evolution of the kinetic phase is justified by the saturation of the nano ferrite adsorption sites. As soon as the sites are filled by the dy molecules, a liquid solid equilibrium is established. The first rapid evolution corresponds to the external mass transfert while the second is slow and linked to the diffusion phenomenon (internal mass transfert).

Adsorbent Dose The amount of adsorbent is an important parameter that influences the adsorption process. It contributes to know the cost of the process outside from the technical aspect.

The adsorption sites can be optimized by the dose effect of the adsorbent. The results (Fig. 9) show that the adsorption rate increases with increasing NCF dose. This can be explained by increase in the number of adsorption sites with increasing adsorbent amount ($R = 73\%$ for 32 mg L^{-1} of dose). As a result, the fixation of molecules to the pores also continues to increase, but after this fixation, there is a stabilization around an equilibrium concentration. At this time, it is preferable to stop increasing the dose, otherwise there will be a decrease of the concentration in the adsorbent suspension. This will lead to the dispersion of the particles in the aqueous phase. Consequently, the adsorbent surfaces will be more exposed and will facilitate the accessibility of a large number of free sites to molecules which initiales a return phenomenon (desorption). Some authors have attributed this decrease to a desorption of the adsorbed compound due to the increase in inter-particle collisions when the mass of adsorbent increases (Machado et al. 2016; Khan et al. 2018). Other authors explain it by a decrease in the molecular diffusion of the solute when the mass of adsorbent increases. Consequently, the time required to establish equilibrium would be longer (Rapo and Tonk 2021; Lin et al. 2008; Xiaoning et al. 2008).

pH of the System Figure 10 shows the variation in the rate of discoloration as a function of the pH. It can be seen that the best removal rate of the dye by nano cobalt is obtained at pH = 2 showing that the adsorption machanism is favoured in an acid medium. This can be explained by the high acidity resulting in a strong electrostatic attraction between the surface of the positivity charged adsorbent and the AG25 dye which implies a high adsorption. On the other hand, when the pH of the system increases, the number of negatively charged sites increases and the number of positively charged sites decreases, resulting in a decrease of adsorption. Research has shown that the increase in adsorption at low pH depends no only on properties associated with the surface of the adsorbent but also on the structure of the dye.

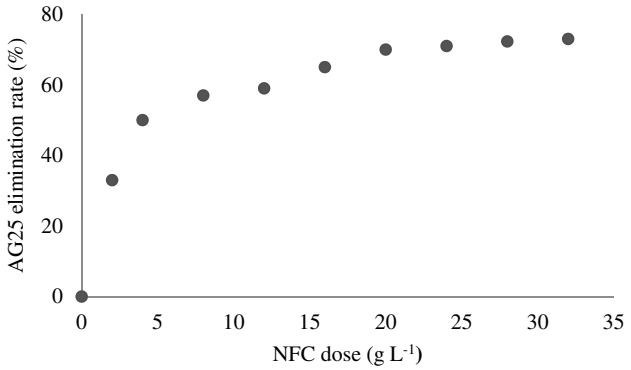

Fig. 9 Discoloration rate of AG25 solution as a function of $CoFe_2O_4$ dose

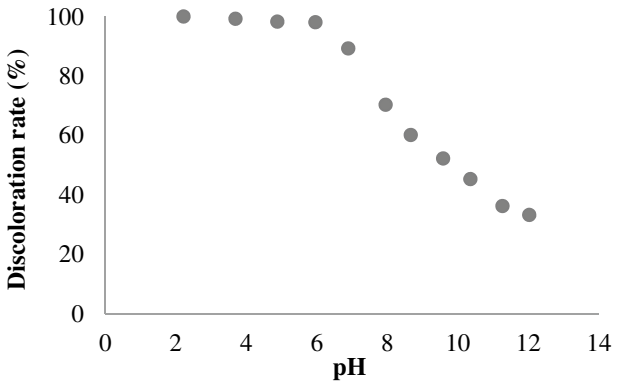

Fig. 10 Discoloration rate of AG25 solution at different pH

Under these conditions a higher adsorption of anionic molecules is favored by an acidic medium. These results corroborate the mechanism proposed in Sect. 3.3.

Adsorption Isotherms

The dye adsorption isotherms of AG25 dye on NCF material is shown in Fig. 11. Adsorption isotherms indicate the distribution of adsorbed molecules between the liquid and solid phases at equilibrium state. The shape of these isotherms can indicate the nature of the interaction between the adsorbate and the adsorbent. It is usually a simple mass transfer process from the liquid phase to the solid surface. According to the IUPAC classification, this isotherm is type I. This type of isotherm is generally obtained in the case of microporous adsorbents with a gradual saturation of the adsorption sites.

The isotherm models can be used to deduce the main characteristic parameters of adsorption.

Many theoretical models have been developed to describe adsorption isotherms. In this work, two types of isotherms models were verified: Langmuir (1918) and Freundlich (1906) models. The first one assumes that the adsorbent surface is

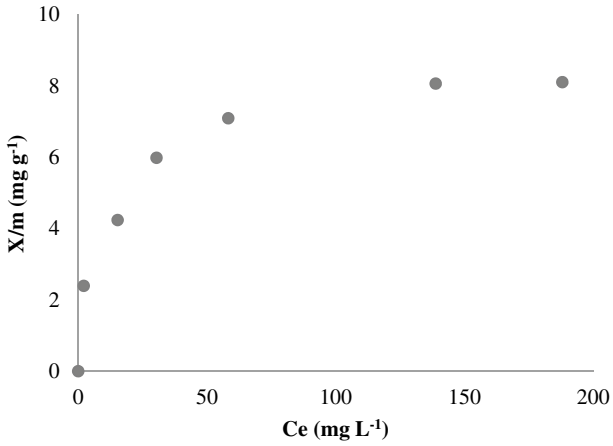

Fig. 11 Adsorption isotherm of AG25 on $CoFe_2O_4$ at 20 °C

uniform with limited adsorption sites. Only a monolayer is created during adsorption and the adsorbate molecules occupy these dictint surface sites without interacting with each other and with identical affinity. The Langmuir equation can be described as follows:

$$q_e = \frac{K_L \times q_{\max} \times C_e}{1 + K_L \times C_e}, \tag{6}$$

where $q_{\max}$ is the adsorbed substrate quantity per solid mass unit (mg g^{-1}), C_e is the AG25 concentration at equilibrium (mg L^{-1}), q_e is the amount of the adsorbed AG25 (mg g^{-1}), K_L is a constant and b is the maximal capacity of adsorption (mg g^{-1}).

Equation (6) can be rearranged as follows:

$$\frac{C_e}{q_e} = \frac{C_e}{q_{\max}} + \frac{1}{K_L q_{\max}}, \tag{7}$$

where $q_{\max}$ and K_L are the constant of the model determined from the curve C_e/q_e versus C_e.

The Freundlich model is the oldest relation describing the adsorption equation. It is often expressed as follows:

$$q_e = K_F C_e^{1/n}, \tag{8}$$

where q_e is the amount of AG25 adsorbed per unit mass of nano ferrite (mg g^{-1}) at equimibrium, C_e is the equilibrium concentration dy in solution (mg L^{-1}). K_F is a Freundlich constant representing the adsorption capacity, n is the adsorption constant intensity and $(1/n)$ is associated to the surface heterogeneity (Meroufel et al. 2015).

Equation (8) can be linearized acconrding the following equation:

$$\ln q_e = \ln K_F + \frac{1}{n} \ln C_e, \tag{9}$$

where K_F and $1/n$ are determined from plotted $\ln q_e$ versus $\ln C_e$.

Figure 12 shows the linearized form of isotherm adsorption according the two mentioned models. The results summarized in Table 2, showed high values of the regression coefficient R^2 (0.9855) for the Langmuir model compared to the Freundich model (0.7498). The slope and the intercept determine the maximum adsorption capacity q_{max} as well as the constant K_L for the nano ferrite adsorbent. The dye adsorption capacity obtained by the nano ferrite has been 8.71 mg of AG25 per gram of material which is encouraging for the improvement of the overall adsorption capacity. It can be concluded that the surface of adsorbent is homogeneous and that the adsorption process of AG25 produces a monolayer on its outer surface because the q_{max} value predicted by the Langmuir model is close to the experimental value (Boamah et al. 2014).

Table 6 summarizes the adsorption capacities of AG25 by $CoFe_2O_4$ and by other materials. A simple comparison between these adsorbents in terms of maximum adsorption capacities, it is possible to classify $CoFe_2O_4$ in the category of Polyaniline/sawdust composite, PANI NT, and PAC-MnO_2-NC. The other materials have certainly much higher capacities but remain recommended for the treatment of aqueous solutions with a high organic matter content.

An essential characteristic of the Langmuir isotherm can be expressed in terms of a dimensionless separation factor or equilibrium parameter R_L. (Hall et al. 1966; Kalotra et al. 2021). The R_L value can be used to indicate the behavior and evaluate the feasibility of the adsorption process. R_L values are given below:

$$R_L = \frac{1}{1 + K_L C_0}, \tag{10}$$

where C_o is the initial concentration of the adsorbate (mg L^{-1}) and K_L the Langmuir constant (L mg^{-1}).

Four scenarios are probable: (i) the adsorption is unfavourable ($R_L > 1$), (ii) the adsorption is favourable ($0 < R_L < 1$), (iii) The adsorption is linear ($R_L = 1$), and finally (iv) the adsorption is irreversible ($R_L = 0$).

According to Fig. 13, there is a favourable adsorption process. Indeed, in the case of the adsorption of AG25 by NFC, the values found from the Langmuir model for R_L were 0.00205, 0.00103, 0.000686, 0.000514, 0.000343 and 0.000294 for the initial concentrations of 50, 100, 150, 200, 250, 300 and 350 mg L^{-1} of AG25, respectively. The confirmed magnetic properties of NFC seem improve the migration of dye molecules into the crystal grains of the material. The AG25 molecule and through its sulphonate groups and under the effect of the concentration gradient migrates to the outer surface of the grain of cobalt nono-ferrites. The loss of a magnetic field within the grains induces an electric field which attracts more the molecule of the dye inside the pore. This mechanism confirms the idea that the material used has both magnetic and electronic characteristics.

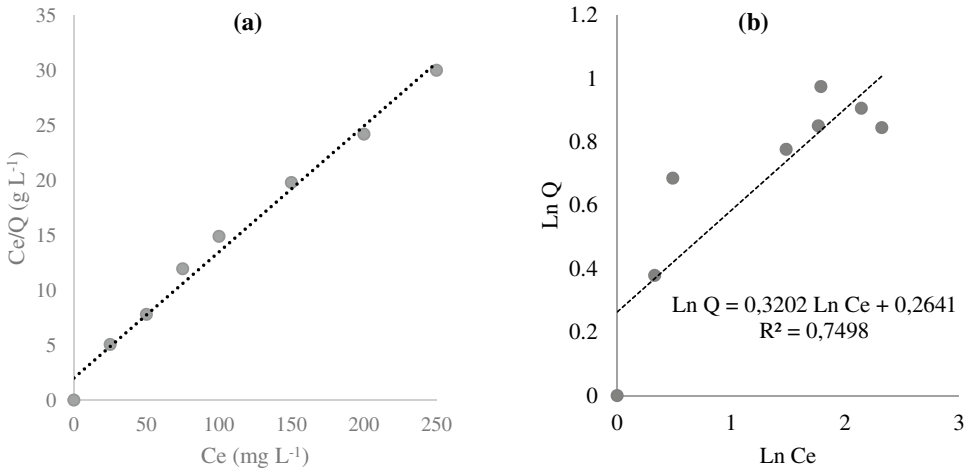

Fig. 12 Adsorption isotherm models: **a** Langmuir; and **b** Freundlich

Table 2 Site occupancy factors and Rietveld parameters

Atom	Wyckoff	S.O.F	$x=y=z$	Rietveld	Parameters	Cations distribution	
O	32e	1.000	0.249	**R_{exp} (%)**	2	**Site A**	**Site B**
Fe(A)	16c	0.680	0.000	**R_{wp} (%)**	3		
Co(A)	16c	0.320	0.000	**GoF**	2	**$Co_{0.36}$ $Fe_{0.64}$**	**$Co_{0.64}$ $Fe_{1.36}$**
Fe(B)	8b	0.640	0.375	**U**	0.249		
Co(B)	8b	0.360	0.375	**a(Å)**	8.321		

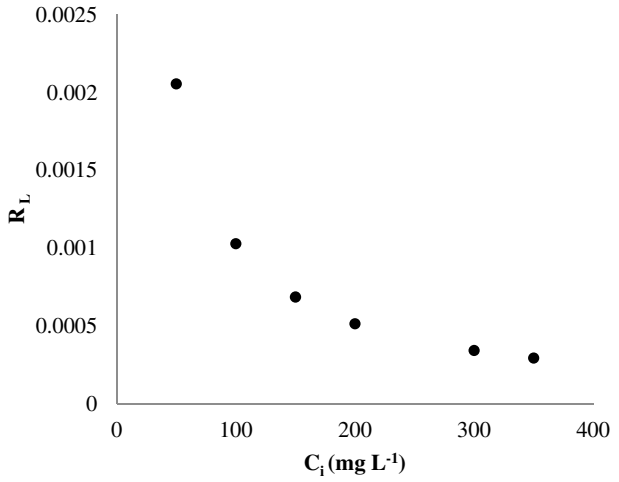

Fig. 13 R_L values according Langmuir model

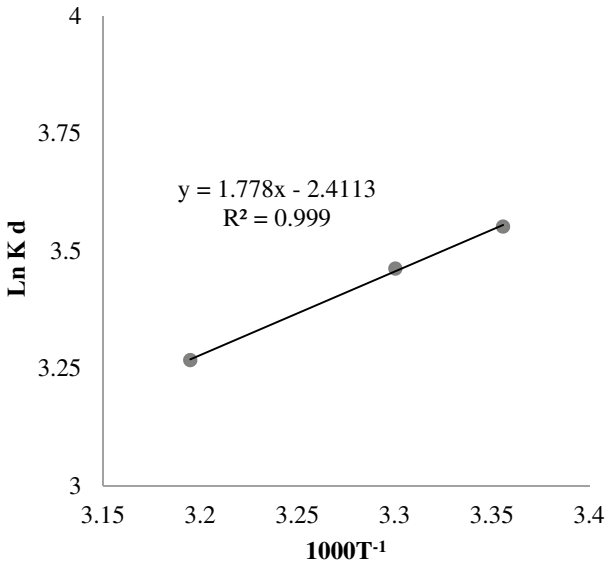

Fig. 15 Evolution of (Ln K_d) vs (1000 T^{-1})

As regards to the Freundlich isotherm model, the parameter n can be used to know the nature of adsorption. If $n = 1$, the adsorption is linear, if $n > 1$, the process is pysical and if $n < 1$, the adsorption process is chemical. In this work, the value of n is greater than 1 (3.12), indicating that the adsorption onto the material surface is a physical process (Ansari et al. 2016).

Adsorption Kinetic

The adsorption process can be known by studing the kinetics of the adsorption rate of AG25 on the adsorbent surface at different contact times (1–120 min). The result obtained were applied to the two most commonly used models: pseudo-first order (Lagergren 1898; Ho and Mcka 1998).

The pseudo-first order model is given by the following equation:

$$\ln\left(q_e - q_t\right) = \ln q_e - k_1 t. \tag{11}$$

The pseudo-second order model is given as follows:

$$\frac{t}{q_t} = \frac{1}{k_2 q_e^2} + \frac{1}{q_e} t, \tag{12}$$

where q_e is the amount of dye adsorbed at equilibrium time (mg g^{-1}), q_t is the quantity of dye adsorbed at time (mg g^{-1}), k_1 is the rate constant of the pseudo-first order, k_2 is the

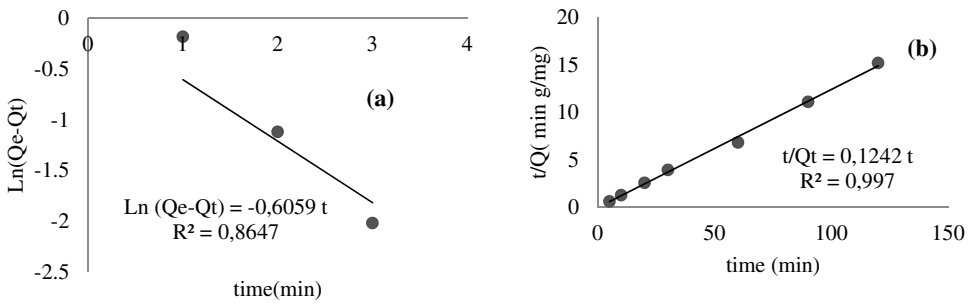

Fig. 14 Kinetics of adsorption process: **a** pseudo-first order; and **b** pseudo-second order

Table 3 Isotherms parameters of adsorption of AG25 by nano-ferrite

Langmuir isotherm parameters			q_{exp} (mg/g)	Freundlich isotherm parameters		
q_m (mg/g)	K_L (L mg^{-1})	R^2		n	K_F (mg g^{-1})	R^2
7.35	9.71	0.9855	8.06	3.12	1.30	0.7498

Table 4 Kinetic parameters of adsorption of AG25

Pseudo-second-order kinetic parameters			q_{exp} (mg/g)	Pseudo-first-order kinetic parameters		
q_{cal} (mg/g)	K_2 (mg/(g.min))	R^2		q_{cal} (mg/g)	K_1 (1/min)	R^2
8.06	0.97	0.997	8.71	2.07	0.91	0.864

Table 5 Thermodynamic parameters of adsorption of AG25 by nano-ferrite as various temperature

Adsorbant	ΔH^0 (kJ mol^{-1})	ΔS^0 (kJ mol K^{-1})	ΔG^0 (kJ mol^{-1})		
Nano-ferrite	− 14.78	− 20.04	298 K	303 K	313 K
			− 8.79	− 8.72	− 8.50

pseudo-second order rate constant (g mg^{-1} min^{-1}) and $h = k_2 q_e^2$ is the initial rate constant (g mg^{-1} min^{-1}).

The order of the the adsorption reaction of the dye on the adsorbent was determined by successively introducing 25 ml of the dye solution of known concentration (30 mg L^{-1}) to which the optimal dose of the adsorbent was added. The mixture is stirred for intervals of less than the equilibrium time. The filtrate is centrifuged and analyzed spectrophotometrically. The results are shown in Fig. 14a and b. In this context, the adsorption of AG25 by cobalt nano ferrite follows pseudo-second order kinetics with $R^2 = 0.997$ and experimental adsoprtion capacity of 8.71 mg g^{-1} near the calculated value of 8.06 mg g^{-1} as it is show in Table 3.

The pseudo-second order model assumes that a first rapid reaction reaches equilibrium very quickly, followed by a second slow reaction that can continue over time. The high value of K_2 (0.96) versus K_1 (0.91) confirms this process of AG25 adsorption by NCF (Zamani and Tabrizi 2014; Hameed et al. 2007).

Adsorption Thermodynamic Parameters

Temperature is an important parameter in the adsorption process. The thermodynamic parameters make it possible to know the nature of the adsorption process and to evaluate the effect of the temperature on the adsoprtion of the dye to the surface on the adsorbent. The effect of temperature on the adsorption was estimated by determining the Gibb's free energy variation ΔG^0, standard enthalpy variation ΔH^0 and standard entropy variation ΔS^0. The Langmuir isotherm was used to calculate the thermodynamic parameters and were obtained from experimental data at temperatures 298 K, 303 K and 313 K using the following equations:

$$\Delta G^{\circ} = \Delta H^{\circ} - T \times \Delta S^{\circ}, \tag{13}$$

$$\Delta G^{\circ} = -R \times T \times \mathrm{Ln} K_d, \tag{14}$$

where ΔG^0 (kJ mol^{-1}) is the Gibb's free energy variation, ΔH^0 (kJ mol^{-1}) is the standard enthalpy variation and ΔS^0 (kJ mol^{-1} K^{-1}) is the standard entropy variation, K_d is the distribution coefficient, R is the universal gas constant (8314 J mol^{-1} K^{-1}) and T (K) is the absolute temperature of the solution.

The results show that the thermal effect did not improve the adsorption capacities. The increase in temperature does not favour the adsorption of the dye by the nano ferrite. The molecules of AG25 tend to leave the solid phase and pass into the solution. This means that the adsorption of AG25 by NCF is favourable at low temperatures. ΔH^0 and ΔS^0 were determined from the slope and intercept of the Van't Hoff curves of (ln K_d) versus (1000/T) (Fig. 15) taking into account the relationship between ΔG^0 and K_d (Eq. 14). The results thus calculated are given in Table 4. The thermodynamic parameters reveals that adsorption of AG25 onto NCF is a spontaneous and feasible process (négative ΔG^0). The $\Delta S^0 < 0$ indicates that the adsorption decreases randomly at the adsorbent-adsorbate interface. The negative ΔH_0 value shows that the adsorption of AG25 in exothermic process. The low value of the activation energy ΔH^0 (− 14.78 kJ mol^{-1}) was below 40 kJ mol^{-1} confirming the physisorption process as reported in the literature (Abechi

Table 6 Maximum adsorption capacities of acid green 25 dye by some adsorbents

Adsorbent	Q_m (mg g^{-1})	References
Polyaniline/sawdust composite	6.21	Ansari and Dezhampanah (2013)
PANI NT	6.89	Ayad and Abu El-Nasr (2012)
PAC-MnO2-NC	9.38	Sathya et al. [2018]
Shells of bittim	16	Aydin and Baysal (2006)
Polyaniline/clay nanocomposites	34.14	Kalotra and Mehta (2021)
Graphene impregnated with MnO_2	324.26	Yusuf et al. (2020)
Self-floating adsorbent	344.8	An et al. (2021)
$CoFe_2O_4$	8.71	**This study**

2018; Edokpayi and Makete 2021). In this case, rate of ΔH^0 coincides with the physorption range. In this way, adsorption of AG25 on the nano ferrite is physical in nature. Although in physical adsorption, the adsorbate species are adsorbed in a short period of contact time, whereas chemical adsorption requires a longer contact time at equilibrium (Dogan et al. 2007; Abechi 2018) (Tables 5, 6).

Conclusion

In the present work, the removal of AG25 in aqueous solution using $CoFe_2O_4$ as an adsorbent was investigated. Cobalt nano-ferrite has been synthetized from aqueous solution by the auto-combustion method and characterized by XRD, SEM, VSM, FTIR spectroscopy and pH_{pzc}. The equilibrium adsorption data can be fitted to the Langmuir isotherm. From this model, the maximum monolayer adsorption capacity for AG 25 was of 8.71 mg g^{-1}. The effect of adsorbent dose, contact time, initial dye concentration, initial solution, pH and temperature of AG25 solution, on adsorption were investigated. The kinetics data were better fitted in the pseudo-second order model from the values of regression coefficient (R^2). The determination of the thermodynamic parameters showed that the process was exothermic, spontaneous and of physisorption nature and partially chemical adsorption.

The combination between results of adsorption process and the proved magnetic properties, a mechanism was proposed to confirm that $CoFe_2O_4$ material has both magnetic and electronic characteristics which can be beneficial for water pollution control. Thus, $CoFe_2O_4$ material can be considered as an efficient adsorbent, low cost, easily synthesized and environmentally friendly for the removal of AG25 from wastewater.

Acknowledgements This research did not receive any specific grant from funding agencies in the public, commercial, or not-for-profit sectors. This work was supported by agrant from the Directorate General for Scientific Research and Technological Development (DG-SRTD), Ministry of Higher Education and Scientific Research ofAlgeria.

Declarations

Conflict of Interest The authors declare that they have no conflicts to interest.

References

Abechi SE (2018) Studies on the mechanism of adsorption of methylene blue onto activated carbon using thermodynamic tools. Sci World J 13(2):17–19

Akhtar MN, Sulong AB, Akhtar MN, Khan MA (2018) Systematic study of Ce^{3+} on the structural and magnetic properties of Cu nanosized ferrites for potential applications. J Rare Earths 36:156–164. https://doi.org/10.1016/j.jre.2017.09.003

Akhtar N, SyakirIshak MI, Bhawani SA, Umar K (2021) Various natural and anthropogenic factors responsible for water quality degradation: a review. Water 13(19):2660. https://doi.org/10.3390/w13192660

An Y, Xiao P, Zheng H, Zhao R, Han M, Mao W, Li Y (2021) Multifunctionalized self-floating microspheres for dyes capture: Amphoteric adsorption and rapid surface solid-liquid separation. J Clean Prod 296:126535. https://doi.org/10.1016/j.jclepro.2021.126535

Ansari R, Dezhampanah H (2013) Application of polyaniline /sawdust composite for removal of acid green 25 from aqueous solutions: kinetics and thermodynamic studies. Eur Chem Bull 2(4):220–225. https://doi.org/10.17628/ECB.2013.2.220

Ansari SA, Khan F, Ahmad A (2016) Cauliflower leave, an agricultural waste biomass adsorbent and its application for the removal of MB dye from aqueous solution. Int J Anal Chem ID 8252354:1–10. https://doi.org/10.1155/2016/8252354

Aragaw TA, Bogale FM (2021) Biomass-based adsorbents for removal of dyes from wastewater: a review. Front Environ Sci 9:764958. https://doi.org/10.3389/fenvs.2021.764958

Ayad MM, Abu El-Nasr A (2012) Anionic Dye (Acid Green 25) Adsorption from Water by using polyaniline nanotubes salt/silica composite. J Nanostruct Chem 3:3. https://doi.org/10.1186/2193-8865-3-3

Aydin H, Baysal G (2006) Adsorption of acid dyes in aqueous solutions by shells of bittim (Pistacia khinjuk Stocks). Desalination 196(1–3):248–259. https://doi.org/10.1016/j.desal.2005.11.025

Baig N, Kammakakam I, Falath W (2021) Nanomaterials: a review of synthesis methods, properties, recent progress, and challenges: a review. Mater Adv 2:1821–1871. https://doi.org/10.1039/D0MA00807A

Benyekhou N, Ghezzar MR, Abdelmalek F, Addou A (2020) Elimination of paracetamol from water by a spent coffee grounds biomaterial. Environ Nanotechnol Monit Manag 14:100396. https://doi.org/10.1016/j.enmm.2020.100396

Boamah PO, Zhang Q, Hua M, Huang Y, Liu Y, Wang W, Liu Y (2014) Lead removal onto cross-linked low molecular weight chitosan pyruvic acid derivatives. Carbohydr Polym 110:518–527. https://doi.org/10.1016/j.carbpol.2014.03.034

Carolin CF, Kumar PS, Saravanan A, Joshiba GJ, Naushad M (2017) Efficient techniques for the removal of toxic heavy metals from aquatic environment: a review. J Environ Chem Eng 5(3):2782–2799. https://doi.org/10.1016/j.jece.2017.05.02911

Cullity BD (1978) Elements of X-ray diffraction, 2nd edn. Addison-Wesley Pub-lishing Company Inc, p 338

Cullity BD, Graham CD (2009) Introduction to magnetic materials, 2nd edn. Wiley, New Jersey

Cullity BD, Stock SR (2013) Elements of X-ray diffraction, 3rd edn. Pearson New Int

Dogan M, Ozdemir Y, Alkan M (2007) Adsorption kinetics and mechanism of cationic methyl violet and methylene blue dyes onto sepiolite. Dyes Pigments 75(3):701–713. https://doi.org/10.1016/j.dyepig.2006.07.023

Edokpayi JN, Makete E (2021) Removal of Congo red dye from aqueous media using Litchi seeds powder: equilibrium, kinetics and thermodynamics. Phys Chem Earth 123:103007. https://doi.org/10.1016/j.pce.2021.103007

Fast SA, Gude VG, Truax DD, Martin J, Magbanua BS (2017) A critical evaluation of advanced oxidation processes for emerging contaminants removal. Environ Process 4:283–302. https://doi.org/10.1007/s40710-017-0207-1

Freundlich HMF (1906) Ober die adsorption in losungen. J Phys Chem A 57:385–470

Gherca D, Cornei N, Mentré O, Kabbour H, Daviero-Minaud S, Pui A (2013) In situ surface treatment of nanocrystalline MFe2O4 (M = Co, Mg, Mn, Ni) spinel ferrites using linseed oil. Appl Surf Sci 287:490–498. https://doi.org/10.1016/j.apsusc.2013.10.018

Hall K, Eagleton L, Acrivos A, Vermeulen T (1966) Pore and solid diffusion kinetics in fixed-bed adsorption under constant-pattern conditions. Ind Eng Chem Fundam 5:212–223

Hameed BH, Din ATM, Ahmad AL (2007) Adsorption of methylene blue onto bamboo-based activated carbon: kinetics and equilibrium studies. J Hazard Mater 141(3):819–825. https://doi.org/10.1016/j.jhazmat.2006.07.049

Hassan MR, Aly MI (2021) Adsorption studies of Eu(III) ions from aqueous solutions by a synthesized copper magnetic ferrite nanoparticles as low-cost adsorbent. J Mater Sci 32:19248–19263. https://doi.org/10.1007/s10854-021-06445-w

Ho YS, McKa G (1998) Kinetic models for the sorption of dye from aqueous solution by wood. Process Saf Environ Prot 76B:183–191

Hossain MSI, Sarker MKR, Khan F, Khan A, Kamruzza M, Rahman MM (2018) Structural, magnetic and electrical properties of sol–gel derived cobalt ferrite nanoparticles. Appl Phys A 124:608. https://hal-amu.archives-ouvertes.fr/hal-02366403

Kadirvelu K, Kavipriya M, Karthika C, Radhika M, Vennilamani N, Pattabhi S (2003) Utilization of various agricultural wastes for activated carbon preparation and application for the removal of dyes and metal ions from aqueous solutions. Bioresour Technol 87:129–132. https://doi.org/10.1016/s0960-8524(02)00201-8

Kalotra S, Mehta R (2021) Synthesis of polyaniline/clay nanocomposites by in situ polymerization and its application for the removal of Acid Green 25 dye from wastewater. Polym Bull 78:2439–2463. https://doi.org/10.1007/s00289-020-03222-3

Kefeni KK, Mamba BB, Msagati TAM (2017) Application of spinel ferrite nanoparticles in water and wastewater treatment: a review. Sep Purif Technol 13872:399–422. https://doi.org/10.1016/j.seppur.2017.07.015

Khan MI, Ansari TM, Zafa S, Buzdar AR, Khan MA, Mumtaz F, Prapamonthon P, Akhtar M (2018) Acid green-25 removal from wastewater by anion exchange membrane: adsorption kinetic and thermodynamic studies. Membr Water Treat 9(2):79–85. https://doi.org/10.12989/mwt.2018.9.2.079

Kosmulski M (2017) The pH dependent surface charging and points of zero charge. VII. Update. Adv Colloid Interface Sci. https://doi.org/10.1016/j.cis.2017.10.005

Kumar M, Dosanjh HS, Singh J, Monir K, Singh H (2019) Review on magnetic nano ferrites and their composites as an alternative in Waste Water Treatment: synthesis, modifications and applications. Environ Sci Water Res Technol 6:491–514. https://doi.org/10.1039/C9EW00858F

Lagergren S (1898) Zur theorie der sogenannten adsorption gelöster stoffe. Kungliga Svenska Vetenskapsakademiens Handlingar 24(4):1–39

Langmuir I (1918) The adsorption of gases on plane surfaces of glass, mica and platinum. J Am Chem Soc 40:1361–1403

Ledakowicz S, Pa´zdzior K (2021) Recent achievements in dyes removal focused on advanced oxidation processes integrated with biological methods. Molecules 26(1–45):870. https://doi.org/10.3390/molecules26040870

Lellis B, Zani C, João FP, Pamphile A, Polonio JC (2019) Effects of textile dyes on health and the environment and bioremediation potential of living organisms: a review. Biotechnol Res Innov 3(2):275–290. https://doi.org/10.1016/j.biori.2019.09.001

Lin JX, Zhan SL, Fang MH, Qian XQ, Yang H (2008) Adsorption of basic dye from aqueous solution onto fly ash. J Environ Manag 87:193–200. https://doi.org/10.1016/j.jenvman.2007.01.001

Machado FM, Sophia AC, Lima EC, Dias SL, Prola PO, Saucier LDT, Jauris C, Zanella IM, Fagan I, SB (2016) Adsorption of alizarin red S dye by carbon nanotubes: an experimental and theoretical investigation. J Phys Chem C 120(32):18296–18306. https://doi.org/10.1021/acs.jpcc.6b03884

Mahmoodi NMM, Taghizadeh A, Taghizadeh M (2018) Mesoporous activated carbons of low-cost agricultural bio-wastes with high adsorption capacity: preparation and artificial neural network modeling of dye removal from single and multicomponent (binary and ternary) systems. J Mol Liq 269:217–228. https://doi.org/10.1016/j.molliq.2018.07.108

Mahmoodi NMM, Taghizadeh M, Taghizadeh A (2019) Activated carbon/metal-organic framework composite as a bio-based novel green adsorbent: preparation and mathematical pollutant removal modelling. J Mol Liq 277:310–3222. https://doi.org/10.1016/j.jenvman.2018.12.026

Manimozhi V, Saravanathamizhan R, Sivakumar EKT, Jaisankar V (2020) Adsorption study of heavy metals removal from wastewater using PVA-nano ferrite composites. Int J Nanosci Nanotechnol 16(3):189–200

Manju G, Mathangi J, Raji P, Kalavathy H (2019) Equilibrium and kinetic studies on methylene blue adsorption by simple polyol assisted wet hydroxyl route of $NiFe_2O_4$ nanoparticles. J Environ Health Sci Eng 17:539–547. https://doi.org/10.1007/s40201-019-00368-9

Mathew DS, Juang RS (2007) An overview of the structure and magnetism of spinel ferrite nanoparticles and their synthesis in microemulsions. Chem Eng J 29:51. https://doi.org/10.1016/j.cej.2006.11.001

Meroufel B, Zenasni MA, Merlin A, George B (2015) Biosorptive removal of zinc from aqueous solution by algerian calotropis procera roots. J Environ Prot 6:735–743. https://doi.org/10.4236/jep.2015.67067

Moosavi S, Lai CW, Gan S, Zamiri G, Pivehzhani OA, Johan MR (2020) Application of efficient magnetic particles and activated carbon for dye removal from wastewater. ACS Omega 5:20684–20697. https://doi.org/10.1021/acsomega.0c01905

Mostafa YN, Mai K (2016) Cobalt ferrite nanoparticles via a template-free hydrothermal route as an efficient nano-adsorbent for potential textile dye removal. RSC Adv 6:79688–79705. https://doi.org/10.1039/C6RA12852A

Murugesan C, Perumal M, Chandrasekaran G (2014) Structural, dielectric and magnetic properties of cobalt ferrite prepared using auto combustion and ceramic route. Physica B 448:53–56. https://doi.org/10.1016/j.physb.2014.04.055

Naseri MG, Saion B, Kamali A (2012) An overview on nanocrystalline $ZnFe_2O_4$, $MnFe_2O_4$, and $CoFe_2O_4$ synthesized by a thermal treatment method. Int Sch Res Notices. https://doi.org/10.5402/2012/604241

Noh JS, Schwarz JA (1989) Estimation of the point of zero charge of simple oxides by mass titration. J Colloid Int Sci 130(1):157–164

Pai S, Kini SM, Narasimhan MK, Pugazhendhi A, Selvaraj R (2021) Structural characterization and adsorptive ability of green synthesized Fe_3O_4 nanoparticles to remove Acid blue 113 dye. Surf Interfaces 23:100947. https://doi.org/10.1016/j.surfin.2021.100947

Pal P (2017) Industry specific water treatment: case studies. In: Industrial water treatment process technology. Butterworth-Heinemann, Oxford, pp 243–511

Prabagar CJ, Anand S, Asisi M, Janifer SP, Materials (2021) Structural and magnetic properties of Mn doped cobalt ferrite nanoparticles synthesized by sol–gel auto combustion method. Mater Today. https://doi.org/10.1016/j.matpr.2021.04.209

Qin H, Hu T, Zhai Y, Lu N, Aliyeva J (2020) The improved methods of heavy metals removal by biosorbents: a review. Environ Pollut 258:113777. https://doi.org/10.1016/j.envpol.2019.11377712

Qu Y, Yang H, Yang N, Fan Y, Zhu H, Zou G (2006) The effect of reaction temperature on the particle size, structure and magnetic

properties of coprecipitated $CoFe_2O_4$ nanoparticles. Mater Lett 60:3548. https://doi.org/10.1016/j.matlet.2006.03.055
Raghasudha M, Ravinderb D, Veerasomaiah P (2015) Electrical resistivity studies of Cr doped Mg nano-ferrites. Mat Discov 2:50–54. https://doi.org/10.4028/www.scientific.net/SSP.241.69
Rápó E, Tonk S (2021) Factors affecting synthetic dye adsorption; desorption studies: a review of results from the last five years (2017–2021). Molecules 26(17):5419. https://doi.org/10.3390/molecules26175419
Rezai B, Allahkarami E (2021) Soft computing techniques in solid waste and wastewater management. In: Chapter 2—wastewater treatment processes—techniques, technologies, challenges faced, and alternative solutions, pp 35–53. https://doi.org/10.1016/B978-0-12-824463-0.00004-5
Sabri K, Rais A, Taibi K, Moreau M, Ouddane B, Addou A (2016) Structural Rietveld refinement and vibrational study of $MgCrxFe^{2-}\ xO_4$ spinel ferrites. Phys B 501:38–44. https://doi.org/10.1016/j.physb.2016.08.01110.1016/j.physb.2016.08.011
Sajjia M, Oubaha M, Hasanuzzaman M, Olabi AG (2014) Developments of cobalt ferrite nanoparticles prepared by the sol–gel process. Ceram Int 40(1):1147–1154. https://doi.org/10.1016/j.ceramint.2013.06.116
Samoila P, Cojocaru C, Cretescu I, Stan CD, Nica V, Sacarescu L, Harabagiu V (2015) Nanosized spinel ferrites synthesized by sol-gel autocombustion for optimized removal of azo dye from aqueous solution. J Nanomater. https://doi.org/10.1155/2015/713802
Saravanathamizhan R, Perarasu VT, Dhandapani B (2021) Advanced oxidation process for effluent treatment in textile, pharmaceutical, and tannery industries. Curr Trends Future Perspect. https://doi.org/10.1016/B978-0-12-823876-9.00020-2
Sathya M, Kumar PE, Santhi M, Muralidharan B (2018) Removal of acid green 25 dye by using activated carbon prepared from *Passiflorafoetida* [Pac-Mno2-Nc] nanocomposite in batch adsorption-kinetic study. Rasayan J Chem 11(4):1741–1749. https://doi.org/10.31788/RJC.2018.1144029
Shen X, Gao X, Wei W, Zhang Y, Ma L, Liu H, Han R, Lin J (2021) Combined performance of hydroxyapatite adsorption and magnetic separation processes for Cd(II) removal from aqueous solution. J Dispers Sci Technol 42(5):664–676. https://doi.org/10.1080/01932691.2019.1703734
Sickafus KE, Wills JM, Grimes NW (1999) Structure of spinel. J Am Ceram Soc 82:3279–3292
Singh M, Dosanjh HS, Singh H (2016) Surface modified spinel cobalt ferrite nanoparticles for cationic dye removal: kinetics and thermodynamics studies. J Water Process Eng 11:152–161. https://doi.org/10.1016/j.jwpe.2016.05.006
Smith J, Wijn HP (1959) Spinel ferrites. Philips Tech, Lib., Eindhoven Holland
Soltys L, Olkhovyy O, Tatarchuk T, Naushad MU (2021) Synthesis of metal and metal oxide nanoparticles: principles of green. Chem Raw Mater Magnetochem 7:145. https://doi.org/10.3390/magnetochemistry7110145
Soufi A, Hajjaoui H, Elmoubarki R, Abdennouri M, Qourzal S, Barka N (2021) Spinel ferrites nanoparticles: synthesis methods and application in heterogeneous fenton oxidation of organic pollutants: a review. Appl Surface Sci Adv 6:100145. https://doi.org/10.1016/j.apsadv.2021.100145
Thakur A, Kumar P, Thakur P, Rana K, Chevalier A, Mattei JL, Queffélec P (2016) Enhancement of magnetic properties of $Ni_{0.5}\ Zn_{0.5}\ Fe_2O_4$ nanoparticles prepared by the co-precipitation method. Ceram Int 42:10664–10670. https://doi.org/10.1016/j.ceramint.2016.03.173
Varghese AG, Paul SA, Latha MS (2019) Remediation of heavy metals and dyes from wastewater using cellulose-based adsorbents. Environ Chem Lett 17:867–877. https://doi.org/10.1007/s10311-018-00843-z
Wang J, Chen H (2020) Catalytic ozonation for water and wastewater treatment: recent advances and perspective. Sci Total Environ 20(704):135249. https://doi.org/10.1016/j.scitotenv.2019.135249
Xiaoning W, Nanwen Z, Bingkui Y (2008) Preparation of sludge-based activated carbon andits application in dye wastewater treatment. J Hazard Mater 153(1–2):22–27. https://doi.org/10.1016/j.jhazmat.2007.08.011
Young RY (1996) The Rietveld method, 3rd edn. Oxford University Press, Oxford
Young RA, Wiles DB (1982) Profile shape functions in Rietveld refinements. J Appl Cryst 15:430–438
Yusuf M, Song K, Geng S, Fazhi X (2020) Adsorptive removal of anionic dyes by graphene impregnated with MnO_2 from aqueous solution. Colloids Surface 595:124667. https://doi.org/10.1016/j.colsurfa.2020.124667
Zamani S, Tabrizi NS (2014) Removal of methylene blue from water by graphene oxide aerogel: thermodynamic, kinetic, and equilibrium modeling. Res Chem Intermed 41:7945–7963. https://doi.org/10.1007/s11164-014-1868-2
Zaviska F, Drogui P, Mercier G, Blais JF (2009) Advanced oxidation processes for waters and wastewaters treatment: application to degradation of refractory pollutants. J Water Sci 22(4):535–564. https://doi.org/10.7202/038330ar

Authors and Affiliations

Ali Belhaine[1] · Fatiha Abdelmalek[1] · Abdelmadjid Rais[1] · Kamel Taibi[2] · Ahmed Addou[1]

✉ Ahmed Addou
ahmed.addou@univ-mosta.dz

[1] Laboratory of Environmental Science and Valorization, Department of Process Engineering, University Abdelhamid Ibn Badis Mostaganem, BP 188, 27000 Mostaganem, Algeria

[2] Laboratory of Materials Science and Engineering, Department of Materials Sciences, Faculty of Mechanical and Engineering Process, USTHB, Algiers, Algeria